Issues associated with Galilean invariance on a moving solid boundary in the lattice Boltzmann method

Cheng Peng, Nicholas Geneva, Zhaoli Guo, and Lian-Ping Wang

Issues associated with Galilean invariance on a moving solid boundary in the lattice Boltzmann method

Cheng Peng, Nicholas Geneva

Department of Mechanical Engineering, University of Delaware, Newark, DE, 19716-3140, USA

Zhaoli Guo

State Key Laboratory of Coal Combustion, Huazhong University of Science and Technology, Wuhan, P.R. China

Lian-Ping Wang

Department of Mechanical Engineering, University of Delaware, Newark, DE, 19716-3140, USA and
State Key Laboratory of Coal Combustion, Huazhong University of Science and Technology, Wuhan, P.R. China

In the lattice Boltzmann simulations involving moving solid boundaries, the momentum exchange between the solid and fluid phases was recently found to be not fully consistent with the principle of local Galilean invariance (GI) when the bounce-back schemes (BBS) and the momentum exchange method (MEM) are used. In the past, this inconsistency was resolved by introducing modified MEM schemes so that the overall moving-boundary algorithm could be more consistent with GI. However, in this paper, we argue that the true origin of this Violation of Galilean invariance (VGI) in the presence of a moving solid-fluid interface is due to the BBS itself, as the VGI error not only exists in the hydrodynamic force acting on the solid phase, but also in the boundary force exerted on the fluid phase, according to Newton's Third Law. The latter, however, has so far been unnoticed by previously proposed modified MEM schemes. Based on this argument, we conclude that the previous modifications to the momentum exchange method are incomplete solutions to the VGI error in LBM. An implicit remedy to the VGI error in LBM and its limitation are then revealed. To address the VGI error for a case when this implicit remedy does not exist, a new bounce-back scheme based on coordinate transformation is proposed. Numerical tests in both laminar and turbulent flows show that the new scheme can effectively eliminate the errors associated with the usual bounce-back implementations on a no-slip solid boundary and maintain an accurate momentum exchange calculation with minimal computational overhead.

PACS numbers: 47.11.Qr, 47.10.ad

I. INTRODUCTION

In the past thirty years, the lattice Boltzmann method (LBM) has been developed into a viable alternative for solving the Navier-Stokes (N-S) equations governing viscous fluid flows. An important reason for its popularity is its apparent simplicity for handling the no-slip boundary condition within complex geometries, which makes it extremely suitable in simulating particle-laden flows [1–4] and flows through porous media [5–7]. In such simulations, the no-slip boundary condition on moving or fixed (typically curved) solid surfaces is usually realized by a bounce-back scheme, which was first proposed in a simple direct bounce back form [1] and later modified to achieve at least a second-order accuracy on curved boundaries [5, 6, 8, 9]. Also inherited from the gas kinetic theory, the hydrodynamic force acting on a solid body in a LBM simulation can be evaluated by summing the net momentum change between the incident and reflected fluid particles at the boundary nodes during the bounce-back process. This mesoscopic treatment is known as the momentum exchange method (MEM) [1, 10], which is computationally more efficient than its macroscopic counterpart, namely, the stress integration method (SIM), as demonstrated in [10, 11].

While bounce-back schemes together with MEM allow different complex geometries to be implemented in LBM, the existence of potential violation of the Galilean invariance (VGI) in these methods has been exposed both theoretically and numerically [12–16]. By the VGI error, we mean that the physical result of the flow, such as the momentum exchange between solid and fluid phases, could change if a constant translational velocity is added to the entire system. Although it is well known that the Galilean-invariant N-S equations can be derived from the LBM scheme via different methods, *e.g.*, Chapman-Enskog analysis [17], asymptotic expansion [18, 19], and linear analysis [20], these derivations often do not consider the presence of a solid boundary. In LBM, popular solid boundary schemes can be roughly grouped into two categories: 1) constructing the mesoscopic distribution functions at the boundary by, *e.g.*, bounce back rules [1, 5, 6, 8, 9] and by direct formulating from the local fluid pressure, velocity and stress information [21]), 2) satisfying the boundary constraints at the level of the macroscopic or N-S equations (*e.g.*, immersed boundary method (IBM) [22, 23]. For example, the hydrodynamic forces in IBM-LBM are evaluated according to the N-S equations on a set of Lagrangian points attached to the solid surfaces [22, 23]. Such forces are then inverted and interpolated as an effective body force exerting on the fluid phase. Thus, in the second category the Galilean invariance is expected to be preserved; and we will no longer consider this category in our paper.

In the past studies [12–16], the VGI error was attributed to MEM. Therefore, in order to correct the VGI error associated with the treatment of a moving solid boundary, several different modifications of MEM have been proposed to improve or restore Galilean invariance (GI) in the calculation of the hydrodynamic force acting on the solid boundary. To our knowledge, Caiazzo & Junk [12] were among the first to realize the lack of Galilean invariance in the MEM and proposed a corrected MEM by subtracting the link-wise VGI error directly on each link. Such link-wise correction is a brute-force treatment that ensures the error be eliminated on all boundary links. Later, Clausen & Aidun [13] presented a straightforward correction that acts in a node-wise manner for an arbitrarily orientated surface. The node-wise correction is designed to remove the overall VGI error on each boundary node. Compared to the link-wise treatment, the major issue for such node-wise correction is that its performance may be affected by the boundary link configuration. Another problem for both correction methods is that they require the VGI errors be formulated and calculated beforehand so the precise errors can be subtracted in their algorithms. Such calculations of the VGI errors involve certain assumptions (*e.g.*, the system is fully relaxed) and are independent of the flow around, so these corrections may not be accurate. Chen *et al.* [14] proposed a corrected MEM to incorporate the impulsive force [2] when a solid node becomes a fluid node, or vice versa. Although it is not intended to eliminate the VGI error, their treatment has later been interpreted as a link-wise correction that essentially achieves the similar node-wise correction in certain ideal cases [24]. More recently, Wen *et al.* designed a Galilean-invariant momentum exchange method (GIMEM), where the lattice fluid velocity relative to the wall was used to realize node-wise Galilean invariance [15]. Compared with its alternatives, this formulation does not require explicit computation of the VGI error. Since its correction term depends on the flow information, *i.e.*, the boundary distribution functions, this method could potentially work better under insufficient grid resolutions. A similar correction was proposed by Krithivasan *et al.* [16] around the same time. Numerical simulations of both laminar and turbulent particle-laden flows indicate that the above corrected force evaluation schemes in Ref. [12–15] lead to physically correct solid-particle motions [15, 24, 25]. Further details of these methods are discussed in Wen *et al.*'s review article [26].

In this paper, we argue that all the above modifications shall not be considered as complete solutions to the VGI errors in LBM. Their incompleteness can be easily seen by considering Newton's Third Law. Namely, if there exists a VGI error in the hydrodynamic force acting on the solid phase, there must be a corresponding VGI error in terms of interaction force experienced by the fluid phase, with the latter being equal and opposite to the former. However, the latter issue remains essentially unnoticed by all the proposed corrections since none of them changes the core algorithm of LBM, *i.e.*, the evolution of distribution functions near a moving fluid-solid interface. The amount of momentum change in the fluid phase due to the moving solid boundary in LBM is purely determined by the bounce back process which is left unchanged no matter what post-processing modifications are made to the momentum exchange scheme.

In other words, the focus of these modifications is on the evaluation of the hydrodynamic force and torque acting on the solid phase, but ignoring the feedback effect of the fluid phase. Without fixing the VGI error on the fluid phase, the one-way correction on the hydrodynamic force evaluation can lead to the violation of Newton's Third Law. In this regard, the previous modifications to MEM are flawed. We will discuss this issue in detail in Sec. II.

We will reveal in detail later in this paper, for some cases, the VGI error on the fluid may be corrected impulsively through the momentum gain/loss when a given lattice node switches phase, namely, a fluid node becomes a solid node or vise versa. However, in some other cases in which this impulsive fix does not occur, $e.g.$, the case where the wall moves along a fixed line (in 2D) or surface (in 3D) relative to the fixed lattice nodes, the VGI error on the fluid phase is left uncorrected. For such specific situations, the existing bounce back schemes need to be improved to address this issue, which is the main focus of this paper.

The rest of this paper is arranged as follows. In Sec. II, we first demonstrate that the true origin of VGI error lies in the bounce-back scheme (the core algorithm) instead of the momentum exchange method (the post-processing part). Based on this argument, we briefly introduce the previous modified momentum exchange schemes and assess their incompleteness both theoretically and numerically. An implicit remedy to the VGI error in LBM and its limitation are then revealed. To eliminate the VGI error in absence of such remedy, a new boundary scheme is presented to restore GI for both fluid and solid phases. The proposed scheme is validated in Sec. IV, using a Poiseuille flow between two inclined walls, a turbulent channel flow, and a turbulent pipe flow. Finally, the contents of this work are highlighted in Sec. V with a summary of key conclusions.

II. ANALYSIS OF DEVIATIONS FROM THE GALILEAN INVARIANCE IN LBM

In LBM, the mesoscopic fluid-particle distribution function $f_i(\mathbf{x}, t)$ is governed by

$$f_i(\mathbf{x} + \mathbf{e}_i, t + \delta_t) - f_i(\mathbf{x}, t) = \Omega_i, \tag{1}$$

where i refers to a discrete particle velocity $\mathbf{e}_i$, $\mathbf{x}$ and t are discrete node and time, respectively, δ_t is the time step size. The right-hand side (RHS) of Eq. (1) is the collision operator, which can take different forms depending on the specific collision model being chosen. The first typical collision model is the single-relaxation-time (or Bhatnagar-Gross-Krook, BGK) model

$$\Omega_i = -\frac{1}{\tau}\left[f_i(\mathbf{x}, t) - f_i^{(eq)}(\mathbf{x}, t)\right], \tag{2}$$

where τ is a non-dimensional relaxation time that is related to the kinematic viscosity ν as $\nu = c_s^2(\tau - 0.5)\delta_t$, where c_s is the model speed of sound, $f_i^{(eq)}$ is the corresponding equilibrium distribution function. The second commonly used collision model is the multi-relaxation time (MRT) model

$$\Omega_i = -\mathbf{M}^{-1}\mathbf{S}\mathbf{M}\left[f_i(\mathbf{x}, t) - f_i^{(eq)}(\mathbf{x}, t)\right], \tag{3}$$

where $\mathbf{M}$ and $\mathbf{M}^{-1}$ are the transform matrix and its inverse, respectively, that relate the distribution functions with a same number of independent moments. $\mathbf{S}$ is the diagonal matrix that defines the relaxation coefficient of each moment. The macroscopic (continuum) density and fluid momentum are obtained in terms of the zeroth and first-order moments of the distribution functions f_i.

A. Momentum Exchange between Solid and Fluid Phases

As mentioned in the Introduction, in the past, the VGI issue in LBM was dealt with only partially by modifying the momentum exchange method [12–16]. Such modifications impact the solid phase only, without a corresponding effect on the fluid phase. As we shall see shortly, this one-way change is flawed and incomplete. The true origin of the VGI error lies in the inappropriate construction of the unknown distribution functions at boundary points near the moving solid-fluid interface, namely, the bounce-back scheme itself.

To understand our argument more clearly, let us consider a simple case where a fluid flow with some initial momenta is present in a pipe. This flow is decelerated due to the wall drag force. In this case, the only force that changes the total momenta of the fluid is the drag force exerted by the wall $\mathbf{F}'$. Based on the principle of Galilean invariance, the fluid inside the pipe should decelerate at the same rate regardless of the frame of reference used. The total momentum change of the fluid phase between t and $t + \delta_t$ can be formulated as

$$\mathbf{m}(t + \delta_t) - \mathbf{m}(t) = \mathbf{F}'\delta_t. \tag{4}$$

In LBM, the fluid momenta $\mathbf{m}$ are calculated as

$$\mathbf{m}\,(t+\delta_t) = \sum_{\mathbf{x},i} f_i\,(t+\delta_t)\,\mathbf{e}_i, \qquad \mathbf{m}\,(t) = \sum_{\mathbf{x},i} f_i\,(t)\,\mathbf{e}_i \tag{5}$$

where the above summations are over all the lattice directions i and all the fluid node points $\mathbf{x}$ in the volume considered.

When the external body force or mean pressure gradient is absent, we have the following relationship between the post-collision fluid momenta and pre-collision fluid momenta

$$\sum_{\mathbf{x},i} f_i\,(t)\,\mathbf{e}_i = \sum_{\mathbf{x},i} f_i^*\,(t)\,\mathbf{e}_i, \tag{6}$$

where $f_i(t)$ and $f_i^*(t)$ are the pre- and post-collision distribution function at a given time step.

Substitute Eq. (5) and Eq. (6) into Eq. (4), we have

$$\mathbf{F}'\delta_t = \sum_{\mathbf{x},i} f_i\,(t+\delta_t)\,\mathbf{e}_i - \sum_{\mathbf{x},i} f_i^*\,(t)\,\mathbf{e}_i. \tag{7}$$

If we consider the fluid phase as a whole, we note that the inner propagation (or streaming) between two fluid nodes does not change the total momenta of the fluid. The only contribution to the fluid momentum change is governed by the fluid particles incident and reflected off the solid boundary. Therefore, Eq. (7) can be re-written as

$$\begin{aligned}
\mathbf{F}'\delta_t &= \sum_{\text{B links}} \left[f_{\bar{i}}\,(t+\delta_t)\,\mathbf{e}_{\bar{i}} - f_i^*\,(t)\,\mathbf{e}_i \right] \\
&= -\sum_{\text{B links}} \left[f_{\bar{i}}\,(t+\delta_t) + f_i^*\,(t) \right]\mathbf{e}_i.
\end{aligned} \tag{8}$$

where $f_{\bar{i}}(t+\delta_t)\mathbf{e}_{\bar{i}}$ represents the momenta carried by the fluid lattice particles coming from the solid phase, and $f_i^*(t)\mathbf{e}_i$ is the momenta carried by the fluid particles entering the solid phase.

It should be noted that Eq. (8) is a general fact in LBM which does not change regardless the algorithm one uses to evaluate the hydrodynamic force acting on the solid phase. In fact, to satisfy Newton's Third Law, *i.e.*, the force exerted on the fluid phase must be precisely the opposite to the hydrodynamic force $\mathbf{F}$ acting on the solid phase, which leads to

$$\mathbf{F}\delta_t = -\mathbf{F}'\delta_t = \sum_{\text{B links}} \left[f_{\bar{i}}\,(t+\delta_t) + f_i^*\,(t) \right]\mathbf{e}_i. \tag{9}$$

As we shall realize soon, Eq. (9) is simply the summation form of conventional MEM, which accurately describes the momentum exchange between solid and fluid phases. Clearly, we have identified *a fundamental inconsistency* in all the previous studies that modify the conventional MEM in order to restore Galilean invariance, which motivated the current study.

B. The VGI Error in the Momentum Exchange

In this subsection, we shall discuss the Galilean variant issue of momentum exchange between solid and fluid phases and reveal its true origin. Consider a moving solid wall and a lattice node ($\mathbf{x}_b$) next to the solid wall in the fluid domain, as illustrated in Fig. 1. There are several fluid lattice particles sitting at $\mathbf{x}_b$ that will travel along the boundary links, these lattice particles interact with the solid boundary causing momentum exchanges between the solid boundary and the fluid. The net momentum exchange between this fluid node and the wall should be identical whether the whole system is at rest or moving with a constant velocity. This is the principle of Galilean invariance. This fundamental principle must be preserved in any non-accelerating inertial frame of reference.

As we discussed before, the momentum exchange between the fluid at the boundary node point $\mathbf{x}_b$ and solid wall must be

$$\mathbf{F}\,(\mathbf{x}_b)\,\delta_t = -\mathbf{F}'\,(\mathbf{x}_b)\,\delta_t = \sum_{\text{B links}} \left[f_{\bar{i}}\,(t+\delta_t) + f_i^*\,(t) \right]\mathbf{e}_i = \sum_{i=1,5,8} \left[f_{\bar{i}}\,(t+\delta_t) + f_i^*\,(t) \right]\mathbf{e}_i. \tag{10}$$

Here we use the notation $\mathbf{F}(\mathbf{x}_b)\delta_t$ to indicate the momentum change of the solid phase and $\mathbf{F}'(\mathbf{x}_b)\delta_t$ for the momentum change of the fluid phase. Typically, in the bounce-back scheme they are related by

$$f_{\bar{i}}\,(t+\delta_t) = f_i^*\,(t) - \frac{2w_i\rho_0}{c_s^2}\,(\mathbf{e}_i \cdot \mathbf{u}_w) \tag{11}$$
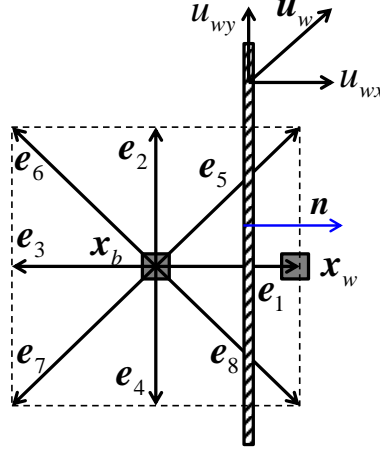
FIG. 1. Configuration of a boundary node that interacts with a moving wall.

where $\mathbf{u}_w$ is the velocity of the solid boundary, and w_i is the weighting factor. Here the incompressible formulation of He & Luo [27] has been adopted, namely, the density is decomposed into a mean reference density ρ_0 and a local fluctuation $\delta\rho$. The second term on the RHS in the above equation approximates the no-slip boundary condition on a moving wall.

In a "fully relaxed system" where the whole flow field is at the same state (*i.e.*, velocity, temperature, etc.) as the solid boundary, we can represent both f_i^* and $f_{\bar{i}}$ with their corresponding equilibrium distributions in terms of the local density fluctuation $\delta\rho$ and velocity $\mathbf{u}_w$ at the wall,

$$f_i^{(eq)} = w_i\delta\rho + \rho_0 w_i \left[\frac{(\mathbf{e}_i \cdot \mathbf{u}_w)}{c_s^2} + \frac{(\mathbf{e}_i \cdot \mathbf{u}_w)^2}{2c_s^4} - \frac{(\mathbf{u}_w \cdot \mathbf{u}_w)}{2c_s^2} \right]. \tag{12}$$

Substituting the equilibrium distribution into the MEM equation, Eq. (9), one can express the momentum exchange as

$$\mathbf{F}\left(\mathbf{x}_b\right)\delta_t = \sum_{\text{B links}} \left\{ 2w_i\mathbf{e}_i\delta\rho + \rho_0 w_i\mathbf{e}_i \left[\frac{(\mathbf{e}_i \cdot \mathbf{u}_w)^2}{c_s^4} - \frac{(\mathbf{u}_w \cdot \mathbf{u}_w)}{c_s^2} \right] \right\}. \tag{13}$$

Assuming a D2Q9 lattice grid and summing over all boundary links in the case of Fig. 1 results in the node-wise momentum exchange as

$$\mathbf{F}\left(\mathbf{x}_b\right)\delta_t = \frac{1}{3}\delta\rho c\mathbf{n} + \frac{\rho_0}{c}u_{wx}\mathbf{u}_w \approx \frac{1}{3}\delta\rho c\mathbf{n} + \frac{\rho_0}{c}\left(\mathbf{u}_w \cdot \mathbf{n}\right)\mathbf{u}_w \tag{14}$$

where $\mathbf{n}$ is the unit wall normal vector ($\mathbf{n} = (1,0)$ in this case) pointing from the boundary fluid node $\mathbf{x}_b$ to the wall surface. The first term on the RHS of Eq. (14) is precisely the hydrodynamic force due to the fluid pressure ($p\mathbf{n}$). Since the system is in a fully relaxed state, this should be the only force acting on the solid boundary. Therefore, the second term on the RHS of Eq. (14), which depends on the wall velocity magnitude u_{wx} and u_{wy}, represents the VGI error in force evaluation, namely,

$$\mathbf{F}_{\text{VGI}}\left(\mathbf{x}_b\right)\delta_t = \frac{\rho_0}{c}\left(\mathbf{u}_w \cdot \mathbf{n}\right)\mathbf{u}_w. \tag{15}$$

It should be noted that the last expression in Eq. (14) is approximate as, due to the discretization and lattice grid layout, the intermediate expression remains correct even the local wall normal deviates slightly from the horizontal direction. Again, it is necessary to emphasize that Eq. (13) is the actual momentum exchange between the fluid at boundary $\mathbf{x}_b$ and the solid wall, which is independent of the scheme that is used to evaluate it. The VGI error exists in both the hydrodynamic force acting on the solid wall as well as the reaction force exerting on the fluid phase. However, in the previous studies [12, 13, 15], the latter has not been realized. The efforts to date have been focused on modifying the force evaluation scheme to enforce the Galilean invariance of the former only. These corrections are thus part of the post-processing, rather are designed to eliminated the VGI error from its true origin. As one could

observe in Eq. (9), the only flexibility that can be taken advantage of to restore Galilean invariance in the momentum exchange between phases is the distribution function $f_{\bar{i}}(t+\delta_t)$ being constructed via the boundary schemes. Therefore, better bounce-back schemes need to be proposed to resolve this issue fully.

C.   Modified Momentum Exchange Methods

For the completeness of our discussion, we shall first review the previous efforts to address the VGI errors, *i.e.*, the improved momentum exchange schemes proposed in Ref. [12–15]. Among these efforts, the schemes of Caiazzo & Junk [12], Clausen & Aidun [13] and Chen *et al.* [14] all require direct computation of the VGI error in terms of distributions under the fully relaxed assumption, so they are discussed together.

Since the momentum exchange between solid and fluid phases should be independent of the wall reference velocity, the velocity-dependent part in Eq. (9) should be viewed as a source for the VGI error and shall be offset in the calculation of hydrodynamic force acting on the solid wall. Starting from that, Caiazzo & Junk [12] proposed a corrected momentum exchange algorithm by directly subtracting the velocity-dependent part out from the momentum exchange to enforce GI on each boundary link, as

$$\mathbf{F}\left(\mathbf{x}_b\right)\delta_t = \sum_{\text{B links}} \left\{ \left[f_{\bar{i}}\left(t+\delta_t\right) + f_i^*\left(t\right)\right]\mathbf{e}_i - \rho_0 w_i \mathbf{e}_i \left[\frac{\left(\mathbf{e}_i\cdot\mathbf{u}_w\right)^2}{c_s^4} - \frac{\left(\mathbf{u}_w\cdot\mathbf{u}_w\right)}{c_s^2}\right]\right\}. \tag{16}$$

This correction is straightforward to implement. Since GI is enforced on each link, the force evaluation at each node point is expected to have the same property, regardless of the boundary link configuration.

Different from Caiazzo & Junk, Clausen & Aidun [13] designed a modified MEM by correcting the VGI error in the force evaluation in a node-wise manner. In Ref. [13], the node-wise VGI error in Eq. (15), is simply subtracted from the actual momentum exchange, *i.e.*, Eq. (9) to restore Galilean invariance. When the wall is arbitrarily oriented, with $\mathbf{n} = (n_x, n_y)$ where $\mathbf{n}$ is the unit wall normal vector pointing from the boundary fluid node $\mathbf{x}_b$ to the wall surface, the momentum exchange evaluated by Clausen & Aidun's modified scheme can be approximately as

$$\mathbf{F}\left(\mathbf{x}_b\right)\delta_t = \sum_{\text{B links}} \left(f_i^* + f_{\bar{i}}\right)\mathbf{e}_i - \frac{\rho_0}{c}\left(\mathbf{u}_w\cdot\mathbf{n}\right)\mathbf{u}_w. \tag{17}$$

It should be noted that in the original formulation proposed by Clausen & Aidun, the term $\delta\rho c\mathbf{n}/3$ in Eq. (14) was also treated as part of the VGI error. However, this term clearly represents the pressure's contribution in the momentum exchange which can be non-zero even if the fluid at $\mathbf{x}_b$ is stationary relative to the wall. Thus, in this paper, this term is not considered as part of the VGI error, contrary to Clausen & Aidun's original proposal.

Alternatively, Chen *et al.* [14] points out that there exists a non-zero fluid mass being displaced by the moving fluid-solid interface in Eq. (11). This displaced fluid mass contains momenta which are ignored in the conventional MEM. Therefore, they corrected the momentum exchange calculation as

$$\mathbf{F}\left(\mathbf{x}_b\right)\delta_t = \sum_{\text{B links}} \left[\left(f_i^* + f_{\bar{i}}\right)\mathbf{e}_i - \frac{2w_i\rho_0}{c_s^2}\left(\mathbf{e}_i\cdot\mathbf{u}_w\right)\mathbf{u}_w\right]$$
$$= \sum_{\text{B links}} \left(f_i^* + f_{\bar{i}}\right)\mathbf{e}_i - \frac{\rho_0}{c}\mathbf{u}_w\sum_{\text{B links}} 6w_i\left(\frac{\mathbf{e}_i}{c}\cdot\mathbf{u}_w\right)$$

where the last term represents the momentum exchange contributed by the displaced fluid mass. It is noted that Chen *et al.*'s method is a link-wise correction. The total amount of correction depends on the boundary link configuration and the last summation in Eq. (18) in general cannot be converted to the form in Eq. (17) or Eq. (16). However, in some ideal cases, for example, a horizontal or a vertical wall, Eq. (16), (17) and (18) become identical. Nevertheless, the correction terms in the above three schemes are very similar in form, and have no dependence on the local flow, *i.e.*, the distribution functions, but is solely determined by the state of the solid phase (and the boundary link configuration in the case of Chen *et al.*). These schemes also require explicit computation of the VGI error under the assumption of a fully relaxed system and simple bounce back rule, *i.e.*, bounce back without interpolation, which could potentially contain numerical errors when an *interpolated* bounce-back scheme is used.

In Ref. [15], a Galilean invariant momentum exchange method (GIMEM) is introduced, and the momentum exchange is computed instead as

$$\mathbf{F}\left(\mathbf{x}_b\right)\delta_t = \sum_{\text{B links}} \left[f_i^*\left(\mathbf{e}_i - \mathbf{u}_w\right) - f_{\bar{i}}\left(\mathbf{e}_{\bar{i}} - \mathbf{u}_w\right)\right]. \tag{18}$$

Their scheme follows a simple physical principle that the momentum exchange between two objects should be expressed based on their relative velocity, in this case, between the fluid lattice particle and the solid boundary, as opposed to the absolute velocity of the lattice particle. Contrary to the schemes in Ref. [12–14], the correction term in this method is related to the actual value of both incident and bounced-back population. Thus the method by Wen *et al.* is arguably more compatible when an *interpolated* bounce-back scheme is used.

We can also compare the correction terms in the above four methods in the limiting case of fully relaxed state in Fig. 1. It is easy to prove the following identities:

$$\mathbf{u}_w \sum_{i=1,5,8} \left(-f_i^* + f_{\bar{i}} \right) = \mathbf{u}_w \sum_{i=1,5,8} \left[-f_i^{(eq)} + f_{\bar{i}}^{(eq)} \right] = -\mathbf{u}_w \frac{\rho_0}{c} \left(\mathbf{u}_w \cdot \mathbf{n} \right)$$

$$= -\frac{\rho_0}{c} \mathbf{u}_w \sum_{i=1,5,8} 6 w_i \left(\frac{\mathbf{e}_i}{c} \cdot \mathbf{u}_w \right) = -\sum_{i=1,5,8} \left\{ \rho_0 w_i \mathbf{e}_i \left[\frac{(\mathbf{e}_i \cdot \mathbf{u}_w)^2}{c_s^4} - \frac{(\mathbf{u}_w \cdot \mathbf{u}_w)}{c_s^2} \right] \right\}. \tag{19}$$

The above discussions show that the four different corrections in the literature, although not identical, are closely related.

However, regardless of what modifications are made, they do not correct the VGI error in the actual momentum exchange between solid and fluid phases, but rather make the expression of hydrodynamic force acting on the solid phase appears to be Galilean invariant. Since these modifications only change the force evaluation on the solid phase, they could potentially break Newton's Third Law, as the force they obtain may not be equal to its opposite force exerting on the fluid phase.

D. An Implicit Remedy of Correcting the VGI Error in LBM

Besides the bounce-back interaction on the fluid-solid surface, the momentum exchange between fluid and solid phases also occurs when a fluid node is covered by a moving solid body or a solid node is uncovered. We will refer to this process as *node-type switching*. When a fluid node becomes a solid node, all the momentum at this node disappears in the fluid domain, which should be converted as a force acting on the solid phase, and vice versa. As we shall see shortly, such impulsive momentum exchange between the two phases can be viewed as a discrete correction to the accumulative VGI errors that takes place continuously. To demonstrate this, let us re-examine the case shown in Fig. 1. Recall Eq. (8), Eq. (15) suggests that there is a VGI error to the fluid phase during each time step, which can be expressed as

$$\mathbf{F}'_{\text{VGI}} \delta_t = -\frac{\rho_0}{c} \left(\mathbf{u}_w \cdot \mathbf{n} \right) \mathbf{u}_w. \tag{20}$$

Assume that the wall moves with constant velocity $\mathbf{u}_w$, this correction shall happen in $c/(\mathbf{u}_w \cdot \mathbf{n})$ time steps before the solid node $\mathbf{x}_w$ on the right is uncovered. The VGI error to the fluid momentum in this process accumulates as

$$\mathbf{M}_{\text{VGI},total} = \mathbf{F}'_{\text{VGI}} \delta_t \cdot \frac{c}{\mathbf{u}_w \cdot \mathbf{n}} = -\rho_0 \mathbf{u}_w. \tag{21}$$

On the other hand, once the node $\mathbf{x}_w$ changes from a solid to fluid node, the distribution functions at this node need to be constructed or initialized. Such reconstruction is also known as the refilling process [24, 28–30]. Due to the constraint of non-slip boundary condition, the velocity at $\mathbf{x}_w$ is expected to be identical with the wall velocity $\mathbf{u}_w$, so the momentum gain for the fluid phase is

$$\mathbf{M}_{\text{gain}} \left(\mathbf{x}_w \right) = \rho_0 \mathbf{u}_w, \tag{22}$$

which cancels precisely with the total VGI error previously accumulated. The same cancellation can be observed when the wall moves in opposite direction and eventually covers the boundary node $\mathbf{x}_b$.

For the fluid phase, such impulsive correction is carried out naturally with a moving solid boundary with respect to the lattice grid itself and provides a self-healing mechanism that maintains the overall Galilean invariance for the fluid phase, over a time scale of the order $c\delta_t/(\mathbf{u}_w \cdot \mathbf{n})$. However, since this self-healing mechanism relies on the solid boundary to physically move with respect to the lattice, covering/uncovering specific nodes, its drawback is obvious. For a flow in which the moving solid boundary does not shift relative to the lattice grid and node-type switching is absent, such as the case where the wall moves along a fixed line (in 2D) or surface (in 3D) relative to the lattice nodes, the VGI error in the fluid phase resulting from the bounce back can no longer be naturally fixed. It is worth pointing out that for the configuration in Fig. 1 (*i.e.*, a flat vertical wall), the VGI error is zero when $u_{wx} = 0$, as indicated by
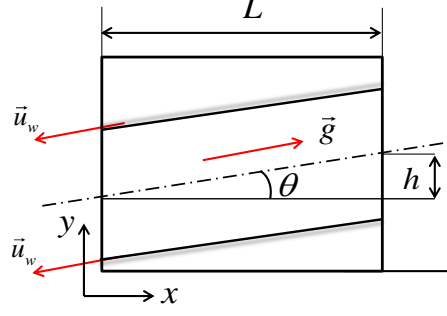
FIG. 2. Sketch of a Poiseuille flow driven by a constant body force between two inclined walls.

Eq. (15). But the VGI error can become non-zero, when the wall is either inclined or curved, or when an interpolated bounce back scheme is needed, as shown by simulation examples below and in Sec. IV.

In order to explicitly demonstrate the VGI error for the fluid phase, we present a simple numerical test case of a Poiseuille flow between two inclined walls driven by a body force. The flow schematic is shown in Fig. 2. Here we choose to make the channel walls inclined, to mimic the more general case of curved boundaries. In the simulations, we set $\theta = \tan^{-1}(1/2)$, $h = 10$, $L = 20$, and the channel width $H = 40$. The fluid is driven by a constant body force to have a centerline velocity $u_c = 0.01$ (relative to the channel walls), in parallel with the channel centerline. The simulation is carried out with a MRT LB model introduced in [20], using the same suggested relaxation parameters for those moments which are irrelevant to the N-S equations. The viscosity is chosen as $\nu = 0.02$. Several simulations were performed, with the walls moving in the direction opposite to the flow driving force, with wall velocity magnitude varying from $u_w = 0.05$ to 0.15. To resolve the solid boundaries with a second-order accuracy, two popular linear interpolated bounce back schemes developed by Bouzidi $et\ al.$ [8] and Yu $et\ al.$ [5] are tested. For completeness of our discussion, the same simulation with the simple bounce back [1] scheme is also presented in parallel. It is noted that, to demonstrate the VGI error on the fluid phase, we purposely introduce a large velocity of the moving frame, relative to the flow velocity change across the channel.

The velocity profiles at the steady state with different wall translation velocities u_w are plotted in Fig. 3. As clearly illustrated in the plots, the velocity profiles with large wall velocity magnitudes deviate significantly from the theoretical result with the two interpolated bounce back schemes. Such results imply that the VGI error introduces additional wall drag to the fluid phase, which causes reduction of the steady-state flow speed. Since, in this case, the solid boundary does not shift with respect to the lattice nodes, the self-healing mechanism previously mentioned is absent in this test case, so that the VGI error accumulates, resulting in reduced overall accuracy of the simulation. On the other hand, the velocity profiles with the simple bounce back scheme do not present significant VGI error, as the profiles with different wall velocities collapse together. When the simple bounce back scheme is employed, the momentum exchange between solid and fluid phases only depends on the information at the boundary nodes, which makes our idealized analysis in Sec. II B applicable. As implied by Eq. (15), in this situation, the VGI error on each link cancels out and results in a negligible error at each boundary node. However, since the simple bounce back has only first-order accuracy, the numerical error due to insufficient discretization is much larger than the two cases with interpolated bounce back schemes. Although the simple bounce back scheme can be viewed as free of VGI error, it is not recommended in the LBM simulations involving complex geometries.

In Table I, we calculate the L1 and L2 error norms of the velocity, which are defined as

$$\varepsilon_{L1} = \frac{\sum_{\mathbf{x}} \mid u_n(\mathbf{x}) - u_t(\mathbf{x}) \mid}{\sum_{\mathbf{x}} \mid u_t(\mathbf{x}) \mid}, \tag{23a}$$

$$\varepsilon_{L2} = \frac{\sqrt{\sum_{\mathbf{x}} \mid u_n(\mathbf{x}) - u_t(\mathbf{x}) \mid^2}}{\sqrt{\sum_{\mathbf{x}} \mid u_t(\mathbf{x}) \mid^2}}, \tag{23b}$$

where u_n and u_t are the numerical and theoretical streamwise velocity, respectively. When the wall velocity is large, the VGI error severely affects the accuracy of LBM simulation when the interpolated bounce back schemes are used. According to our previous analysis in Eq. (20), the magnitude of the VGI error is expected to be on the order of $O(u_w^2)$. In Table I, the L1 and L2 error norms shown in the parentheses are those subtract the corresponding error with $u_w = 0$ and then normalized by $(u_w/u_c)^2$. Indeed, in each case, it is confirmed that the VGI error scales with u_w^2. This feature does not apply very well for the simple bounce back case. For the simple bounce back scheme, the numerical errors are mainly contributed by its intrinsic first-order accuracy. The L1 and L2 norms only have week
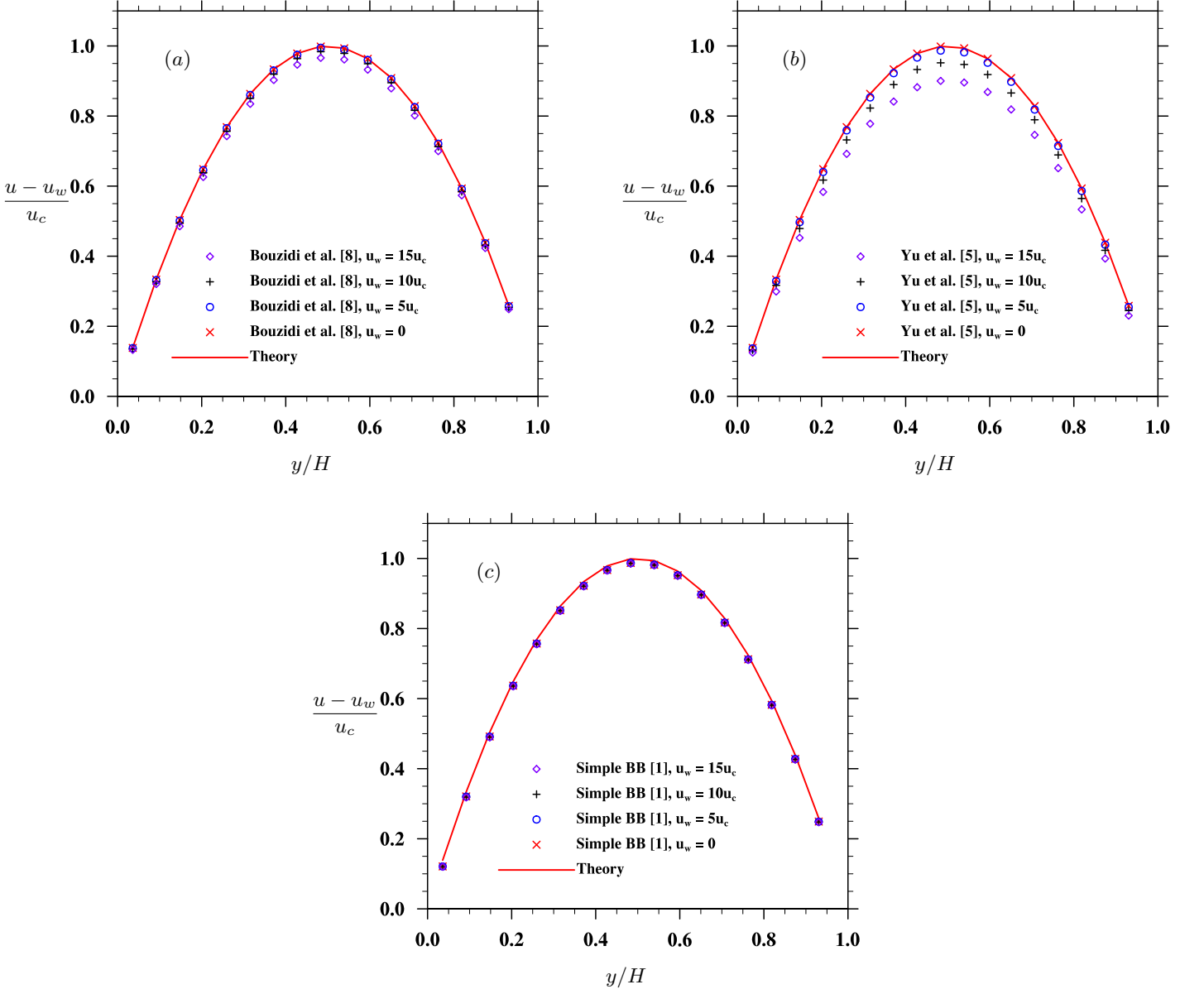
FIG. 3. The steady-state velocity profiles when different reference (moving-wall) velocities are applied: (a), with Bouzidi et $al.$ [8]'s bounce back scheme, (b), with Yu et $al.$ [5]'s bounce back scheme (c), with simple bounce back scheme [1].

dependence on the reference wall velocity.

Fig. 4 shows the total hydrodynamic force $\mathbf{F}$ acting on the two walls with four momentum exchange schemes, $i.e.$, the conventional momentum exchange method, and four modified schemes by Caiazzo & Junk [12], Clausen & Aidun [13], Chen et $al.$ [14], and Wen et $al.$ [15], respectively. The black straight line indicates the total driving force $\mathbf{G}$ applied to the system. When the flow reaches steady state, the total driving force should be balanced with the total drag $\mathbf{F}'$ exerted by the walls, $i.e.$, $\mathbf{G} + \mathbf{F}' = 0$. Additionally, Newton's Third law requires that the hydrodynamic force acting on the wall and drag force acting on the fluid be equal and opposite, $\mathbf{F} = -\mathbf{F}'$, which yields $\mathbf{G} = \mathbf{F}$.

With both bounce back schemes, Wen et al [15]'s one-sided correction fails to satisfy Newton's Third Law. The breakdown of Newton's Third Law originates from the imbalance between Eq. (18) and Eq. (8). On the other hand, the correction terms in Ref. [12–14] vanish due to the fact that both corrections are independent of the local flow and mesoscopic distributions. More specifically, here $\mathbf{u}_w \cdot \mathbf{n} = 0$, Clausen & Aidun [13]'s correction is then zero. Caiazzo & Junk [12]'s and Chen et $al.$ [14]'s corrections are also zero in this case because the link configurations for the top and bottom walls are mirrored. Although the distribution functions at a boundary node near the top wall may be different from the distribution functions at a boundary node near the bottom wall, Both Caiazzo & Junk's and Chen

TABLE I. The L1 and L2 errors for the simulated steady-state velocity field with different bounce back schemes, using various reference velocities.

u_w/u_0	Bouzidi *et al.* [8], ε_{L1}	Bouzidi *et al.* [8], ε_{L2}	Yu *et al.* [5], ε_{L1}	Yu *et al.* [5], ε_{L2}	Simple BB [1], ε_{L1}	Simple BB [1], ε_{L2}
0	8.194E-4	7.528E-4	6.828E-4	6.279E-4	1.760E-2	1.618E-2
5	4.552E-3(1.493E-4)	4.375E-3(1.449E-4)	1.264E-2(4.783E-4)	1.241E-2(4.713E-4)	1.804E-2(1.760E-5)	1.658E-2(1.600E-5)
10	1.600E-2(1.518E-4)	1.565E-2(1.490E-4)	4.815E-2(4.747E-4)	4.770E-2(4.707E-4)	1.916E-2(1.560E-5)	1.761E-2(1.430E-5)
15	3.419E-2(1.483E-4)	3.363E-2(1.461E-4)	1.005E-1(4.436E-4)	9.984E-2(4.409E-4)	2.056E-2(1.316E-5)	1.890E-2(1.209E-5)
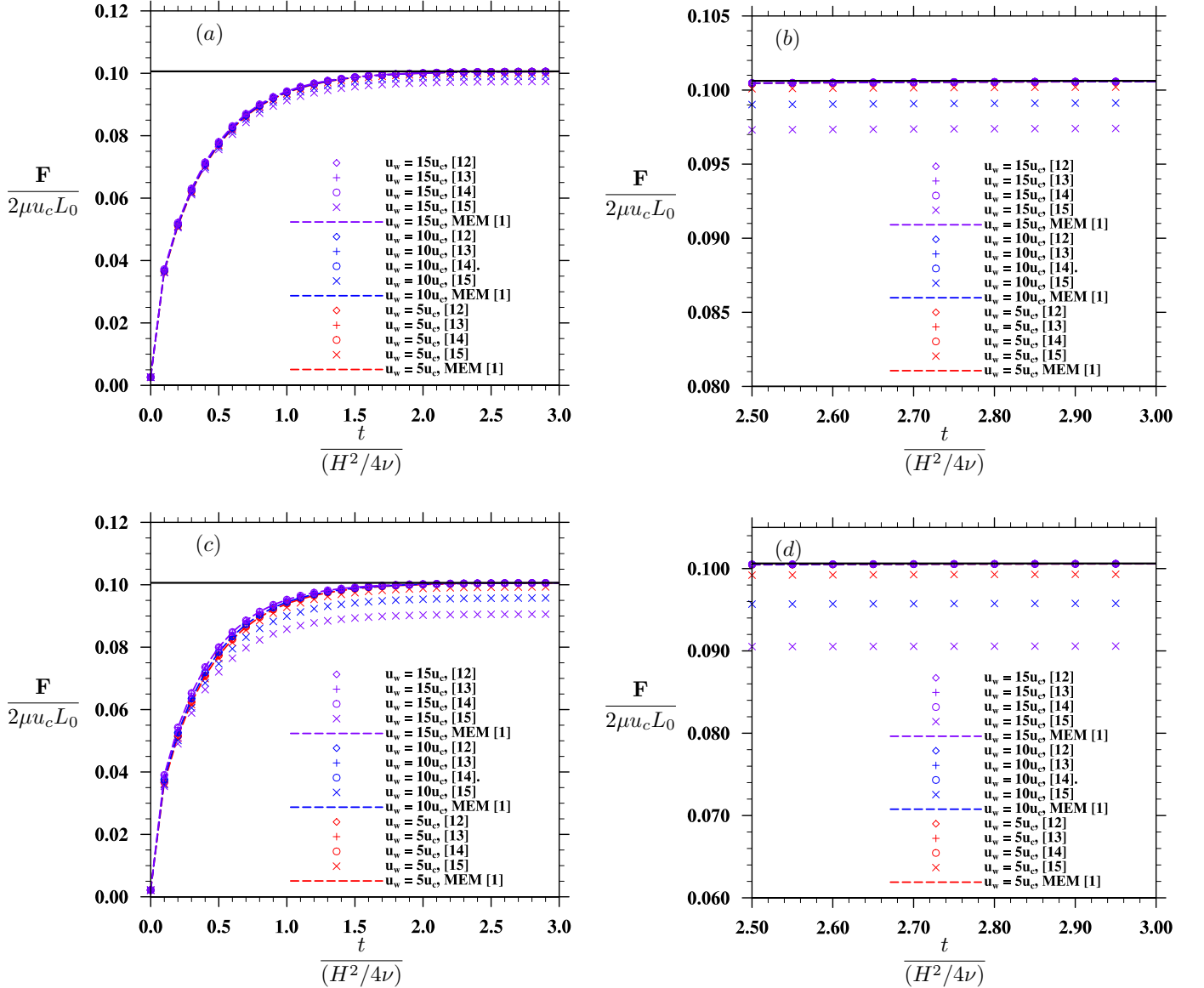
FIG. 4. The time-dependent total hydrodynamic force acting on the two walls calculated with different momentum exchange schemes: (a), with Bouzidi *et al.* [8]'s bounce back scheme; (b), zoom-in plot of (a); (c), with Yu *et al.* [5]'s bounce back scheme; (d), zoom-in plot of (c). $L_0 = \sqrt{h^2 + L^2}$.
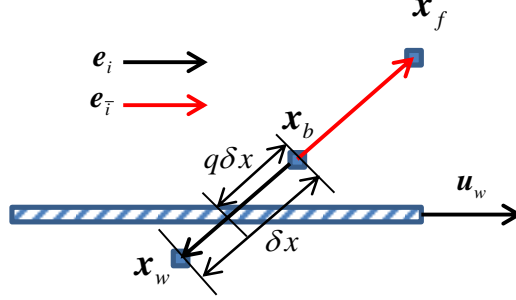
FIG. 5. Sketch of a boundary node that interacts with a moving wall, used to illustrate the new bounce-back implementation.

et al.'s correction terms are not affected by such difference. Therefore, Caiazzo & Junk's, Clausen & Aidun's and Chen *et al.*'s schemes maintain Newton's Third Law in this case. Wen *et al.*'s correction term, however, is affected by this difference in the distribution functions. Thus Wen *et al.*'s scheme violates Newton's Third Law in this case.

III.   A NEW BOUNCE-BACK SCHEME BASED ON COORDINATE TRANSFORMATION

In the previous section, we analyzed the origin of VGI errors for both the solid and fluid phases, along with the previous efforts to restore Galilean invariance on the solid phase. Without a simultaneous correction to the fluid phase, the previous efforts are deemed incomplete. The correction on the fluid phase depends entirely on the details of the bounce-back scheme. When the solid boundary undergoes shifting relative to the lattice nodes, a self-healing mechanism can be triggered as explained in Section 2.3. Although the correction of hydrodynamic force evaluation on the solid phase and the self-healing mechanism on the fluid phase together may not satisfy either Galilean invariance or the Newton's Third Law at each step, they seem to work well when integrated over time, as indicated by the reasonable results of particle dynamics in the previous simulations of turbulent particle-laden flow [14, 15, 24, 25]. The VGI error on the fluid phase does emerge when the moving solid boundary is stationary relative to the lattice nodes and the self-healing mechanism for the VGI error in the fluid phase is not present. Since the boundary force exerted on the fluid is intrinsically determined by Eq. (8), where the only degree of freedom is the bounce-back population $f_{\bar{i}}$, to restore the Galilean invariance, we need to design better boundary schemes.

In this paper, we present a new bounce-back scheme to remove the VGI error when the moving boundary is stationary relative to the lattice nodes, namely, the node-type switching is absent. Our basic idea is to replace the bounce-back in a frame fixed to lattice nodes, to a bounce-back implementation in a frame moving with the wall. This ensures that the bounce-back is always performed in a transformed frame where the wall is static. To achieve this, the distribution functions on the boundary nodes in the transformed frame need to be constructed. In LBM, we can always partition the distribution function f_i into two parts: the equilibrium part $f_i^{(eq)}$ and the non-equilibrium part $f_i^{(neq)}$. The equilibrium part contains information of the conserved quantities (density, momentum) and thus can be calculated directly from the conserved quantities which are known in both frames of reference. On the other hand, the non-equilibrium part contains information of non-conserved quantities (stress, energy flux, *etc.*), which in general can be approximated as functions of only strain rates [21]. Therefore, the non-equilibrium part is not affected by the constant frame velocity or the VGI error. Thus based on this understanding of LBM, we can transform distribution functions between a static frame and a moving frame of reference.

For a boundary configuration shown in Fig. 5, our proposed bounce-back implementation consists of the following steps:

1. After the collision sub-step, starting with the distribution functions in the *fixed* coordinate system (*i.e.*, the coordinate system attached to the lattice grid), we construct the distribution functions in the coordinate system moving with the wall (the *moving* coordinate system), for *all* distribution functions that reach the boundary fluid node $\mathbf{x}_b$ after propagation. These distribution functions include two sets, the distribution functions that arrive $\mathbf{x}_b$ from direct propagation (including the one at rest), and those from bounce-back. For the first group, we have

$$f_i'(t + \delta_t, \mathbf{x}_b) = f_i'^*(t, \mathbf{x}_b - \mathbf{e}_i) \tag{24}$$

where f with superscript prime indicates the distribution functions in the *moving* coordinate system while $*$ indicates the post-collision distribution functions. For the second set of the distribution functions, certain bounce-back scheme is applied. Note here the scheme could be any bounce-back scheme per user's own choice. For demonstration purpose, we use the double linear interpolation scheme proposed by Yu *et al.* [5]

$$f_{\bar{i}}'(t + \delta_t, \mathbf{x}_b) = \frac{q}{1+q} f_i'^*(t, \mathbf{x}_b) + \frac{1-q}{1+q} f_i'^*(t, \mathbf{x}_f) + \frac{q}{1+q} f_{\bar{i}}'^*(t, \mathbf{x}_b) \tag{25}$$

All the involving post-collision distribution functions in the *moving* coordinate system are transformed from the *fixed* coordinate system as

$$f_i'^*(t, \mathbf{x}) = f_i^{(neq),*}(t, \mathbf{x}; \mathbf{u}^*, \delta\rho^*) + f_i^{(eq),*}(t, \mathbf{x}; \mathbf{u}^* - \mathbf{u}_w, \delta\rho^*) \tag{26}$$

where $\mathbf{u}^*$ and $\delta\rho^*$ are post-collision local velocity and density fluctuation at the location $\mathbf{x}$.

2. Next, use $f_i'(t + \delta_t, \mathbf{x}_b)$ to update the density fluctuation and velocity at $\mathbf{x}_b$ in the *moving* coordinate system

$$\delta\rho'(t + \delta_t, \mathbf{x}_b) = \sum_i f_i'(t + \delta_t, \mathbf{x}_b), \qquad \rho_0 \mathbf{u}'(t + \delta_t, \mathbf{x}_b) = \sum_i f_i'(t + \delta_t, \mathbf{x}_b) \mathbf{e}_i. \tag{27}$$

3. Finally, transform *all* distribution functions at $\mathbf{x}_b$ in the *moving* coordinate system back to the *fixed* coordinate system, as

$$f_i(t + \delta_t, \mathbf{x}_b) = f_i'^{(eq)}(t + \delta_t, \mathbf{x}_b; \mathbf{u}' + \mathbf{u}_w, \delta\rho') + f_i'^{(neq)}(t + \delta_t, \mathbf{x}_b; \mathbf{u}', \delta\rho'). \tag{28}$$

Since in Step 3 *all* distribution functions are updated, the momentum exchange between solid and fluid phases at a boundary node obviously contains two parts. The first part is realized via momentum exchange during the bounce back. At the same time, the momentum carried by the direct streaming from the neighboring nodes could also have been modified. This part of momentum change should be taken into consideration in order to obey Newton's Third Law *locally*. In summary, the hydrodynamic force acting on the solid surface should be calculated as

$$\mathbf{F}(\mathbf{x}_b, t)\delta_t = \sum_{\text{B links}} [f_{\bar{i}}(t + \delta_t, \mathbf{x}_b) + f_i^*(t, \mathbf{x}_b)] \mathbf{e}_i + \sum_{\text{others}} [f_i(t + \delta_t, \mathbf{x}_b) - f_i^*(t, \mathbf{x}_b - \mathbf{e}_i\delta_t)] \mathbf{e}_i \tag{29}$$

where the first summation is over the boundary links while the second summation is over the remaining links at $\mathbf{x}_b$.

A few comments can be made for the proposed bounce-back scheme. First, it can be applied to any existed bounce back schemes. Although we illustrate our method with Yu *et al.*[5]'s interpolated bounce-back scheme, the same process can be applied to the other bounce back schemes. Second, this bounce back implementation should *not* be considered as a universal solution for all cases with moving boundaries. When the node-type switching exists (*e.g.*, in a solid-particle suspension), the self-healing mechanism will automatically take care of the VGI error for the moving boundaries, thus this proposed bounce back scheme is arguably unnecessary. Ideally, the bounce back scheme should be designed so it can precisely address the remaining VGI error (if any) when the self-healing mechanism exists. However it is not possible to know the magnitude of the corrections during this process in advance, thus a universal solution is unlikely to exist. In this paper, we constrain ourselves to the cases where the self-healing mechanism is absent. Finally, although similar philosophy of transforming distribution functions between a fixed grid and a moving grid has already been applied in the multi-block technique [31] and immersed boundary method [32], the present scheme still has its own advantages. A second set of grid in the moving frame is unnecessary in the present bounce back scheme. The present bounce-back scheme is only applied to the boundary nodes. Furthermore, for problems that the whole computational domain is attached with a reference velocity, the implementation of multi-block technique or immersed boundary method will be much harder than the present scheme.

IV. NUMERICAL VALIDATIONS

In this section, the proposed bounce back is examined in three test cases without node-type switching: a two dimensional Poiseuille flow between two inclined straight walls (the same case already considered in Section 2, a three dimensional direct numerical simulation (DNS) of a turbulent channel flow and a three dimensional DNS of a turbulent pipe flow.
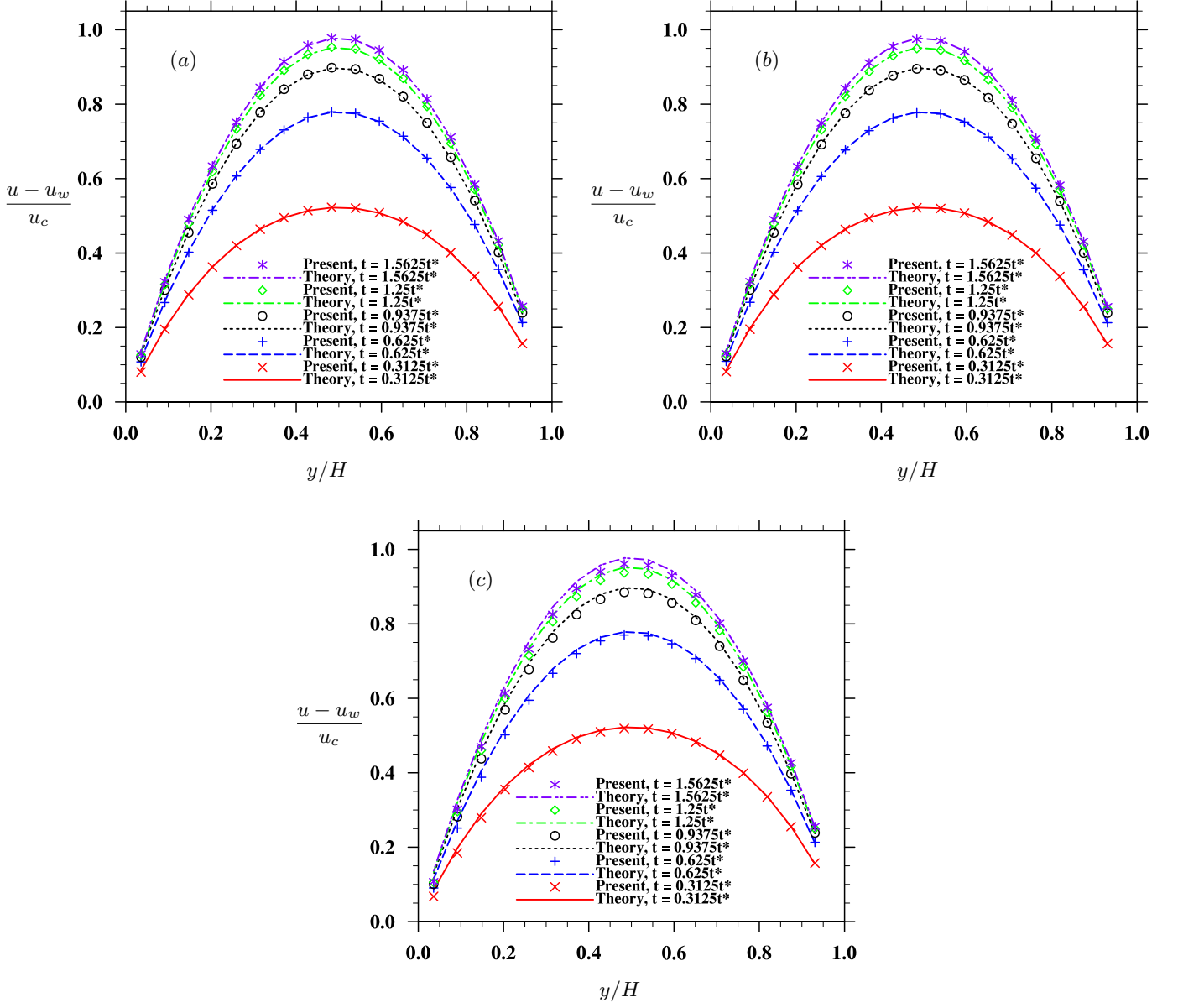
FIG. 6. The velocity profiles at different times using the proposed bounce back scheme with $u_w = 15u_c$: (a), based on Bouzidi *et al.*[8]'s bounce back scheme, (b), based on Yu *et al.*[5]'s bounce back scheme, (c), based on simple bounce back scheme [1]. The dimensionless time is defined as $t^* = H^2/(4\nu)$.

A. A Poiseuille flow between two inclined straight walls

First, the Poiseuille flow between two inclined straight walls, driven by a body force, is tested with the proposed bounce back scheme. As we have demonstrated in Sec. II, due to the VGI error for the fluid phase, the resulting fluid momentum deviates significantly from the theoretical solution. The test runs utilize the same parameter settings as in Sec. II. The proposed bounce back scheme is implemented using both Bouzidi *et al.*[8]'s and Yu *et al.*[5]' bounce back schemes, the corresponding results of velocity profiles with a wall velocity $u_w = 15u_c$ at different times are presented in Fig. 6. For complete assessment, the same results based on the simple bounce back scheme [1] are also provided in parallel.

As shown in Fig. 6, when the interpolated bounce back schemes are used, the velocity profiles at different times collapse well with the corresponding theoretical results, even with this largest wall velocity. This is in contrast with the large derivations in Fig. 3, which indicates that the VGI error has been significantly suppressed with the
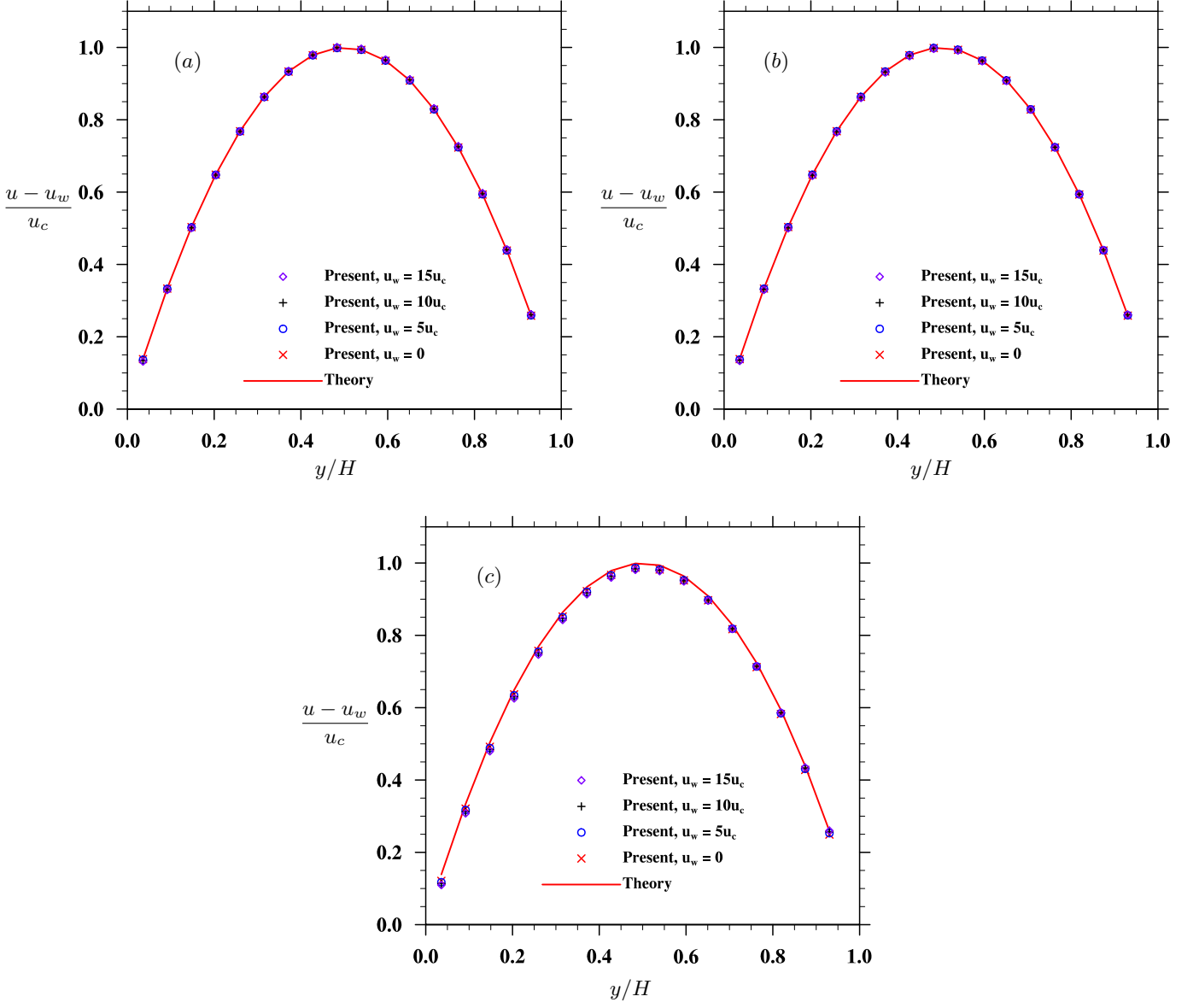
FIG. 7. The steady-state velocity profiles using the proposed bounce-back scheme with different reference velocities: (a), based on Bouzidi *et al.*[8]'s bounce back scheme, (b), based on Yu *et al.*[5]'s bounce back scheme, (c) based on simple bounce back scheme [1].

proposed bounce back scheme. On the other hand, the velocity profiles based on the simple bounce back deviate from the theory at later times, which is mainly due to the first-order accuracy of simple bounce back scheme. Similar to Sec. II, the steady-state velocity profiles with different wall velocities and their error norms are presented in Fig. 7 and Table II, respectively. The values in the parentheses in Table II again represent the error norms after subtracting their corresponding norms with $u_w = 0$ and then divided by $(u_w/u_c)^2$. Compared with the results in Fig. 3 and Table I, we can clearly observe that the proposed bounce back scheme has successfully reduced the error in the velocity calculation by at least one order of magnitude when incorporating the two interpolation schemes. On the contrary, when the simple bounce back scheme is used, the error norms become slightly larger. As we have demonstrated before, the VGI error (if it exists) is not significant with the use of the simple bounce back scheme, which makes our correction arguably unnecessary. Furthermore, unlike the error norms shown in Table I due to VGI, for the two interpolated bounce back schemes, the error norms in Table II no longer scale with $O(u_w^2)$, implying that the majority of the original VGI errors have been eliminated by the proposed coordinate transformation method. For the simple bounce back case, the error norms in the parentheses still scale with $O(u_w^2)$.

TABLE II. The L1 and L2 errors for the simulated steady-state velocity field, using the proposed bounce back rule incorporated with different interpolation schemes.

u_w/u_0	Bouzidi *et al.* [8], ε_{L1}	Bouzidi *et al.* [8], ε_{L2}	Yu *et al.* [5], ε_{L1}	Yu *et al.* [5], ε_{L2}	Simple BB [1], ε_{L1}	Simple BB [1], ε_{L2}
0	8.194E-4	7.528E-4	6.828E-4	6.279E-4	1.763E-2	1.621E-2
5	9.440E-4(4.984E-6)	1.137E-3(1.539E-5)	8.000E-4(4.688E-6)	8.971E-4(1.077E-5)	1.833E-2(2.800E-5)	1.714E-2(3.720E-5)
10	1.888E-3(1.069E-5)	2.091E-3(1.338E-5)	1.848E-3(1.165E-5)	1.974E-3(1.346E-5)	2.038E-2(2.750E-5)	1.974E-2(3.530E-5)
15	3.539E-3(1.209E-5)	3.658E-3(1.291E-5)	3.857E-3(1.411E-5)	3.935E-3(1.470E-5)	2.367E-2(2.684E-5)	2.363E-2(3.298E-5)

The hydrodynamic force as a function of time is shown in Fig. 8, for different wall velocity magnitudes. Due to the consideration of the Newton's Third Law in the proposed method, the hydrodynamic force is clearly equal to the driving force when the flow reaches steady state, as indicated by Fig. 8, for all wall velocity magnitudes tested.

B. Direct numerical simulation of a turbulent channel flow

Next, we apply the new bounce back scheme in direct numerical simulation of fully developed turbulent channel flow. For a boundary node $\mathbf{x}_b$ near a straight channel wall, as shown in Fig. 9, the node-wise VGI error depends on the bounce back scheme being used. When the mid-link bounce back is applied, although a certain VGI error is carried by the bounce back on a single link i, it cancels precisely with the corresponding VGI error carried by link j, as one can prove from Eq. (13). The straight wall guarantees the co-existence of link i and j. When an interpolated bounce back is used, on the other hand, the VGI error carried by a single link not only depends on the information at the boundary node $\mathbf{x}_b$, but also on the extensional node(s) used in the interpolation. Due to the high non-uniformity in the turbulent flow, the information at the two extensional nodes ie and je are unequal, which prevents the VGI errors from precise cancellation. Therefore, the VGI errors may affect the overall results.

Based on the above analysis, our simulation is carried out with the interpolated bounce back. The channel center is purposely shifted by 0.25 lattice spacing to create the need to use an interpolated bounce back to maintain overall second-order accuracy, as shown in Fig. 10. A non-zero wall velocity $u_w = -12u_*$ that is opposite to the driving force direction is added to both walls, where $u_* = \sqrt{\tau_w/\rho}$ is the friction velocity, τ_w is the wall shear stress (per unit area), ρ is the fluid density. The interpolated bounce back scheme of Yu *et al.* [5] and corresponding new bounce back scheme based on the same interpolation strategy are applied to handle the no-slip boundary on the walls. Other than that, the simulation parameters, specific model parameters, initial condition, as well as the method to excite the transition to turbulence are all identical with the case "MRT" as reported in [33].

It is noteworthy that in the direct numerical simulations of high Reynolds number flows, adding a non-zero velocity to the whole system brings a desired benefit of enhancing the numerical stability. For example, with the same simulation set-up, removing the wall velocity can cause severe checkerboard instability in the channel center region which eventually ruins the simulation, as indicated by the pressure contours in Fig. 11. So far we are not sure what exactly triggers the checkerboard instability, but such instability is only observed when the maximum Ma of the flow reaches a certain threshold. For channel flow where the Ma is dominated by the mean velocity in the streamwise direction, we can reduce the maximum Ma at the channel center by adding an opposite velocity ($u_w = -12u_*$ as applied in our simulation) to the system. After adding this constant translation to the system, the simulations with both bounce back rules are stable.

Here we only discuss the average profiles when the flow becomes statistically stationary. The mean velocity profiles on a log-linear plot with both bounce back rules are presented in Fig. 12. To benchmark these profiles, two profiles from pseudo-spectral simulations, denoted by "Stanford" [34] and "Jimenez" [35], as well as our earlier result [33] (denoted by "Wang et al.") based on mid-link bounce back with the same grid resolution are also shown in the same plot. Except the small difference exhibited near the channel center, the profile from the new bounce back matches perfectly with the pseudo-spectral results in most of the region. The small deviation at the channel center may be due to the slight asymmetry in the current simulation or the additional dissipation caused by the interpolation compared to the mid-link bounce back in our earlier study [33]. On the other hand, the mean velocity profile from Yu *et al.*'s original bounce back deviates from the benchmark results significantly due to the VGI errors originated from the boundary. This comparison for the more complex non-uniform unsteady flow clearly indicates that the lack of Galilean invariance in the usual bounce back schemes can lead to erroneous results, and the proposed new implementation can fix this problem.

Fig. 13 and Fig. 14 show the Reynolds stress profiles and the root-mean-square (r.m.s.) velocity profiles, respectively.
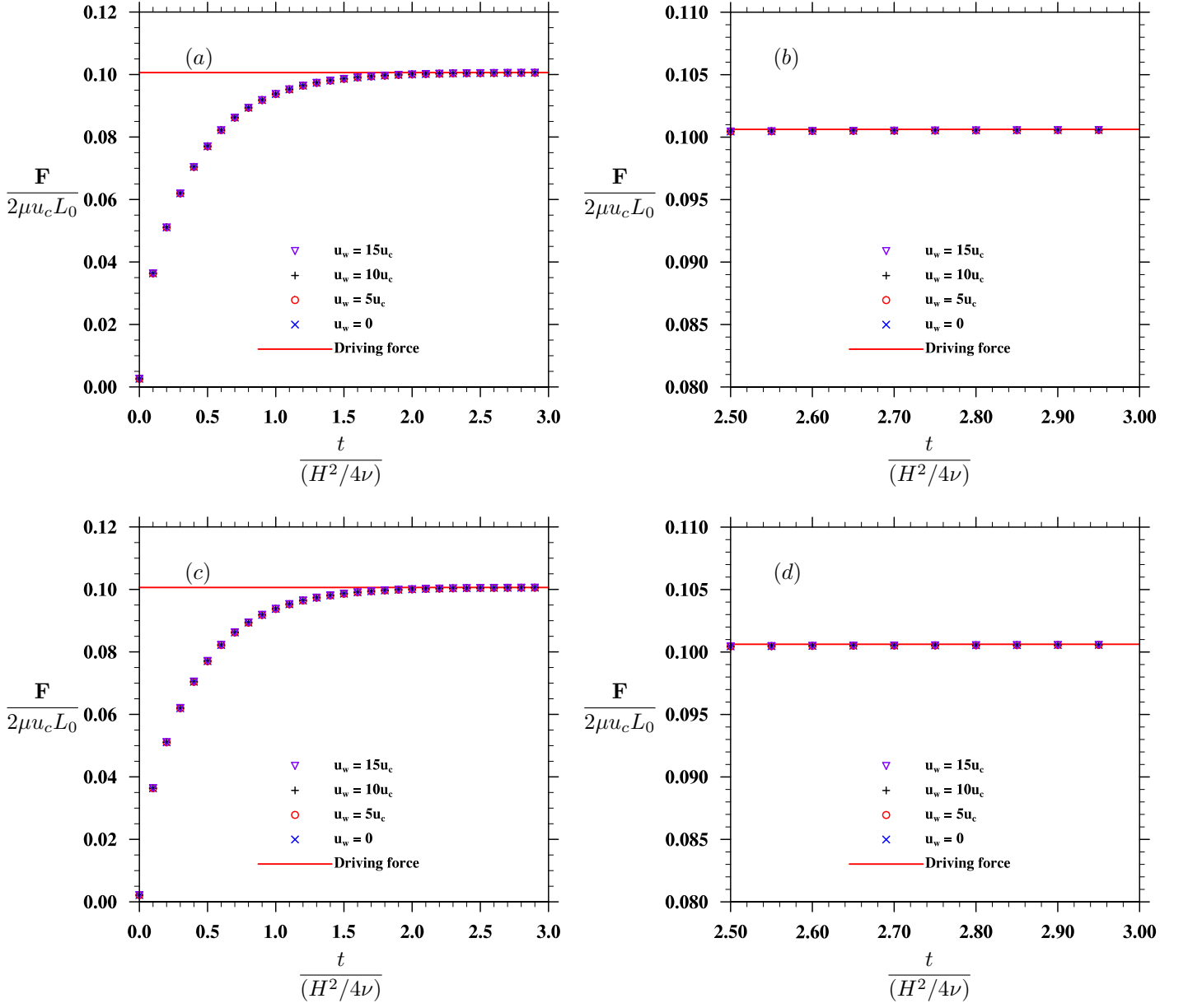
FIG. 8. The time-dependent total hydrodynamic force acting on the two walls with different wall velocities using the proposed bounce back scheme: (a), based on Bouzidi et $al.$[8]'s bounce back scheme; (b) zoom-in plot of (a); (c), based on Yu et $al.$[5]'s bounce back scheme; (d) zoom-in plot of (c). $L_0 = \sqrt{h^2 + L^2}$.

Compared to the mean flow property, the impact of the VGI errors on the velocity fluctuation is relatively small. This might be explained by the fact that the velocity fluctuations in a turbulent flow is more directly associated with the stress components, which are less affected by the VGI errors. Even so, slight improvement is still observed in the Reynolds stress profiles with the new bounce back, when compared with results from Yu et $al.$ [5] 's original interpolated bounce back. The r.m.s. velocity profiles confirm that the results from the new bounce back match better with our earlier LBM results that is free from the VGI errors due to use of the mid-link bounce back, compared to Yu et $al.$'s original scheme.

Finally, at the stationary stage, we calculate the hydrodynamic force on the two walls, normalized by the total driving force. For Yu et $al.$'s bounce back, the hydrodynamic force is evaluated based on both conventional MEM (Eq. (9)) and the GIMEM (Eq. (18)) by Wen et al [15], while for the new bounce back, the force is calculated using Eq. (29). At the stationary stage, the average hydrodynamic force is again expected to be equal to the total driving
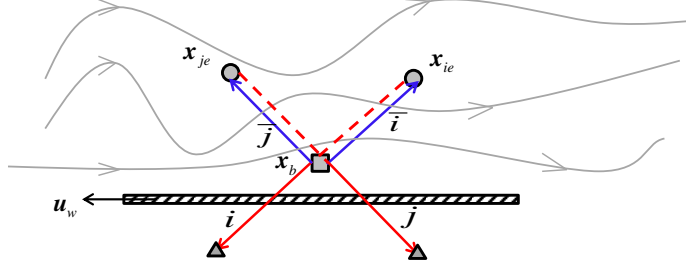
FIG. 9. A sketch of boundary configuration in a turbulent channel flow.
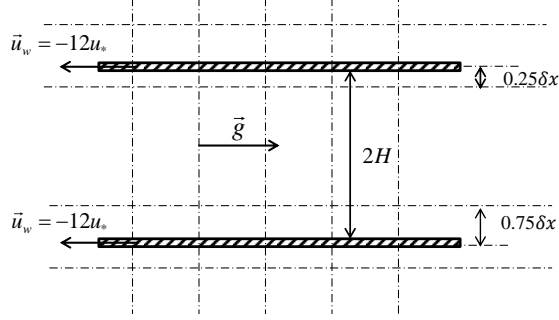

FIG. 10. Grid arrangement in the turbulent channel flow simulation.

force. As shown in Fig. 15, in this case, due to that all boundary nodes have the same set of symmetric boundary links, the correction term in GIMEM is essentially zero. As a result, MEM and GIMEM give identical total hydrodynamic forces when Yu *et al.*'s bounce back is used. In more general cases, for example, with curved boundaries, GIMEM may create a non-zero correction term that leads to the breakdown of Newton's Third Law, as we demonstrated in the case of viscous flow in the inclined channel. We will also confirm such statement in the next section with a direct numerical simulation of turbulent pipe flow. On the other hand, the hydrodynamic force calculation in the new bounce back always satisfies Newton's Third Law, as confirmed by the results shown in Fig. 15. The time-averaged values of the ratio of total hydrodynamic force to total driving force are 0.9962 and 0.9975 for Yu *et al.*'s original bounce and our new bounce back scheme, respectively.

It is worth pointing out that although the new bounce back scheme appears to be much more complicated than its corresponding original bounce back rule, with careful implementation, the computational overhead is negligible since the transformation is done on boundary nodes, which takes only a small portion of the whole domain. In the case of DNS of turbulent channel flow, we use two-dimensional domain decomposition to divide the whole computational domain into 200 sub-domains, the time overhead of our new bounce back scheme is only 1.1% (measured by the wall clock time based on two runs submitted on the same date and finished at about the same time).

C. Direct numerical simulation of a turbulent pipe flow

As a final demonstration, the new bounce back scheme is also examined in our recent direct numerical simulation of a fully developed turbulent pipe flow. For the similar reason as we demonstrated in Sec. IV B, the VGI error carried by each link cannot be cancelled out precisely to restore the overall GI on boundary nodes due to the use of the previous interpolated bounce back schemes that ensures second-order accuracy on boundary treatment. As shown in Fig. 16, the flow in the circular pipe is driven by a constant body force ρg (per unit volume) that maintains a friction Reynolds number $Re_\tau = u_* R/\nu = 180$. Again, a negative (opposite to the driving force direction) wall velocity $u_w = -12u_*$ is added to the pipe wall so the flow speed at the pipe center can be reduced to bring better numerical stability, which was the initial motivation for our development in this paper. On the pipe surface, the interpolated bounce back scheme of Yu *et al.* [5] and its corresponding new bounce back scheme with the same interpolation strategy are tested.

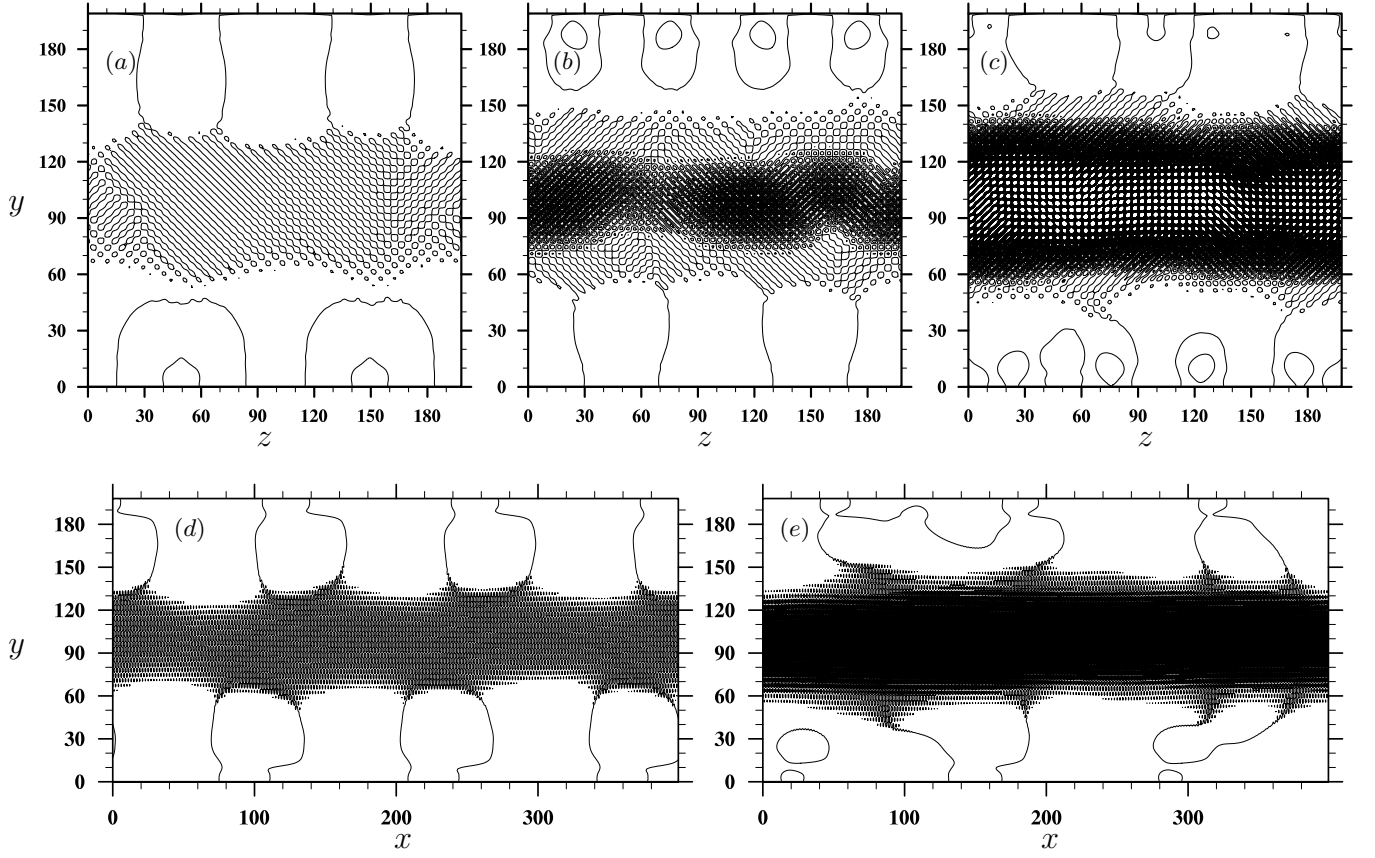The mean flow velocity profiles of both bounce back schemes are presented in Fig. 17 when the flow becomes

FIG. 11. Pressure contours in a turbulent channel flow simulation indicating the existence of checkerboard instability. Top row: pressure contours at a streamwise location $x = nx/2$ at (a) $t = 7,000$, (b) $t = 7,500$ and (c) $t = 8,000$. Bottom row: pressure contours at a spanwise location $z = nz/2$ at (d) $t = 7,000$ and (e) $t = 8,000$.
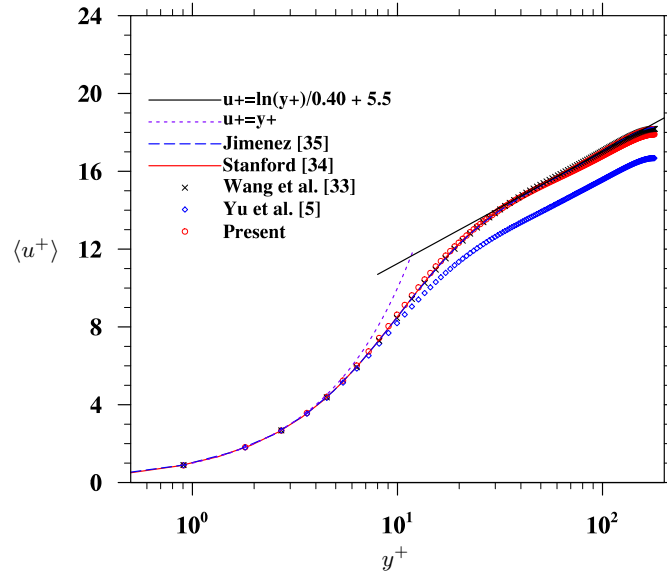

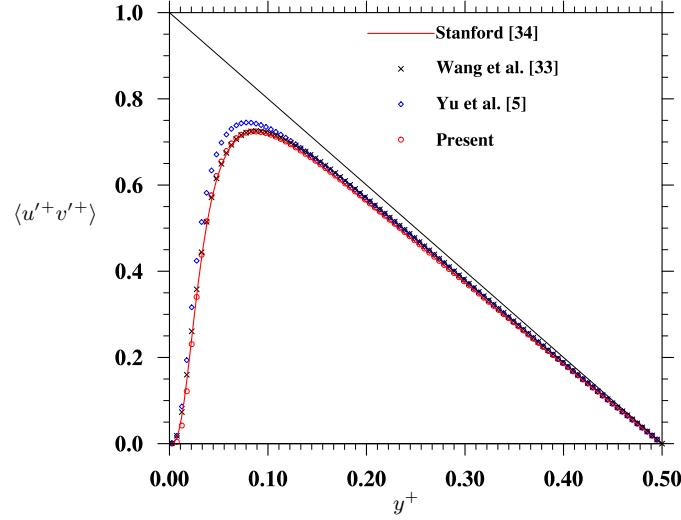FIG. 12. The averaged mean velocity profiles at the stationary stage in the turbulent channel flow simulation.

FIG. 13. The averaged Reynolds stress profiles at the stationary stage in the turbulent channel flow simulation.
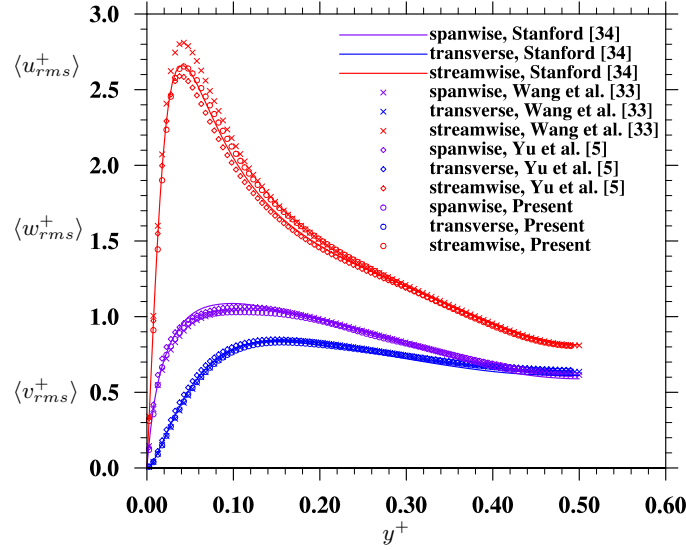
FIG. 14. The averaged r.m.s, velocity profiles at the stationary stage in the turbulent channel flow simulation.

stationary. Here we use the spectral simulations done by Loulou *et al.* [36] with the friction Reynolds number $Re_\tau = 190$ as the benchmark. Although this Re_τ is slightly different from the one in our simulations, its impact on the turbulent statistics is expected to be insignificant. Similar as in the turbulent channel flow case, the mean velocity profile with Yu *et al.*'s original bounce back scheme deviates from the spectral result significantly due to the additional drag caused by the VGI error. On the other hand, our new bounce back scheme successfully eliminates the VGI error and results in a velocity profile that in excellent agreement with the benchmark. The r.m.s. velocity profiles at the stationary stage are shown in Fig. 18. Again, similar as the turbulent channel flow case, the VGI error only has minor effect on the r.m.s velocities in the turbulent pipe flow. This makes sense since the r.m.s. velocities measure the intensity of velocity fluctuation which is independent of reference frame we choose. At last, we examine the hydrodynamic force evaluation at the stationary state to check if the equality between the total driving force and the total hydrodynamic force is well captured, as required by Newton's Third law. Clearly, as shown in Fig. 19, when Yu *et al.*'s bounce back scheme is used, the normalized hydrodynamic force evaluated by MEM oscillates around unity while that calculated by GIMEM is in general smaller than 1. This confirms our statement in Sec. IV B that GIMEM creates non-zero corrections in more general cases that leads to the breakdown of Newton's Third Law. Again, the
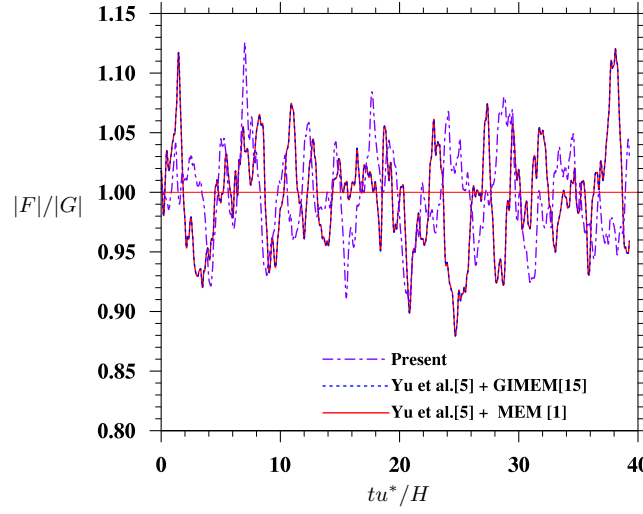
FIG. 15. The normalized total hydrodynamic force acting on the two walls at stationary state in the turbulent channel flow.
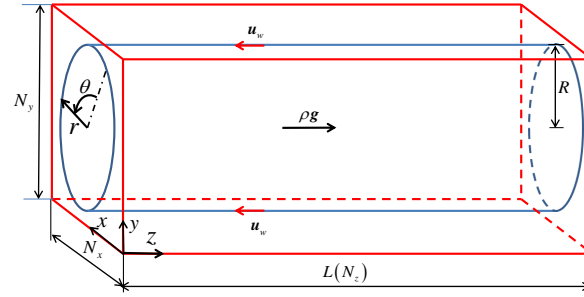

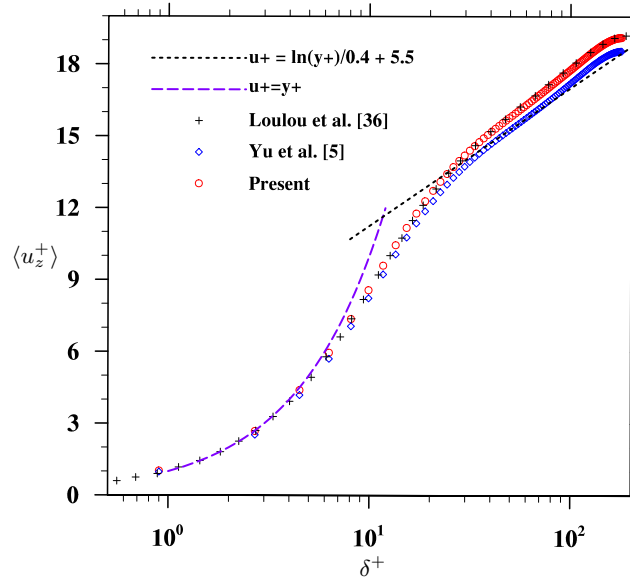FIG. 16. Sketch of the turbulent pipe flow simulation.

FIG. 17. The averaged mean velocity profiles at the stationary stage, relative to the pipe wall, in the turbulent pipe flow simulation.
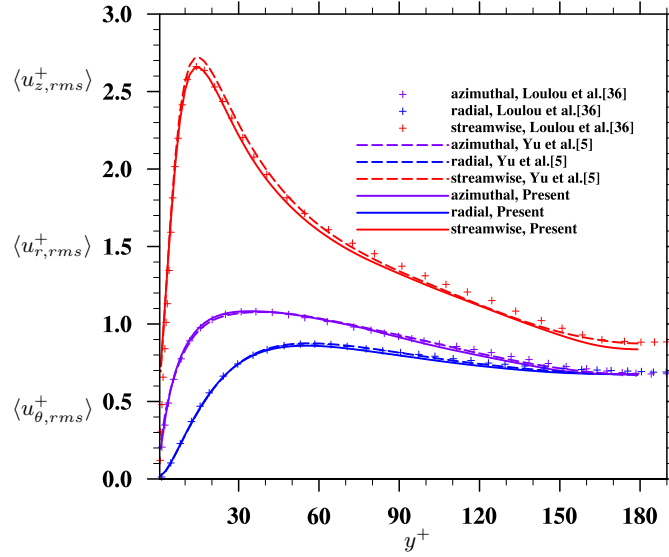
FIG. 18. The averaged r.m.s, velocity profiles at the stationary stage in the turbulent pipe flow simulation.
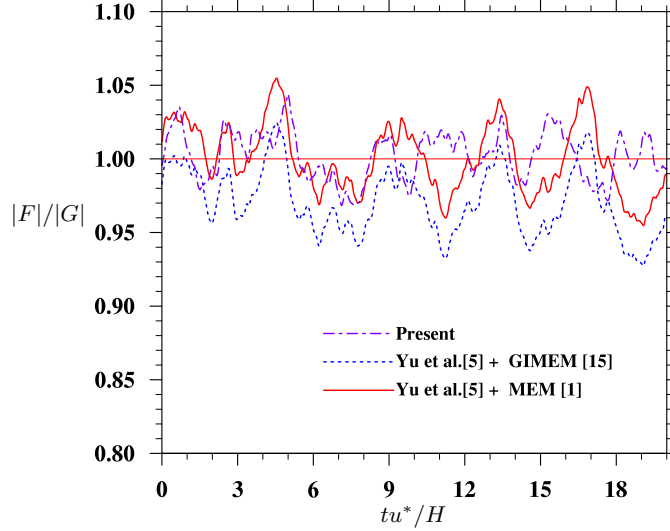

FIG. 19. The normalized total hydrodynamic force acting on the two walls at stationary state in the turbulent pipe flow.

force evaluation in the new bounce back scheme obeys Newton's Third Law well, as the total normalized hydrodynamic force varies around unity. The time-averaged values of the normalized hydrodynamic force are, 1.0004, 0.9709 and 1.0014, for MEM and GIMEM with Yu *et al.*'s bounce back, and the new bounce back scheme, respectively.

V. CONCLUSIONS

In this work, we analyzed the problem of lacking Galilean invariance in the momentum exchange between solid and fluid phases when previous bounce back schemes and momentum exchange method were used. We stressed the need to consider Galilean invariance for both the hydrodynamic force acting on the solid surface and the momentum exchange of the fluid phase due to the fluid-moving wall interaction, as a requirement from Newton's Third law.

Specifically, the main conclusions of this study are summarized below:

1. The lack of Galilean invariance in the force evaluation based on the momentum exchange method has been widely recognized in the recent years. Different modified momentum exchange schemes are proposed to eliminate the

violation of Galilean invariance (VGI) errors in force evaluation on a solid body [12–15]. However, as required by the Newton's Third Law, a corresponding error also exists in the fluid phase. The error in the fluid phase is purely due to the inappropriate construction of the missing distribution functions on a boundary node, which has not been addressed in the previous studies.

2. In the LBM simulations involving solid-fluid interactions, the impulsive momentum exchange between the two phases, taking place when a solid node being uncovered or a fluid node being covered can be viewed as an automatic correction to the VGI error in the fluid phase. However, in the cases without such self-healing mechanism, the VGI error in the fluid phase is intact and can cause severe inaccuracy in the fluid velocity calculations. Furthermore, the one-sided correction of the VGI error on the solid surface, without a simultaneous correction on the fluid phase, could violate Newton's Third Law under certain circumstances. These problems have been demonstrated using LBM simulations of viscous flow in an inclined channel when a significant translational velocity (u_w) is added to the whole system; in this case, we show that the VGI error is proportional to u_w^2. Clearly, this can ruin the default accuracy of LBM, which is know to have an inherent truncation error of $\mathcal{O}(u^3)$.

3. A new bounce back scheme based on the coordinate transformation is then proposed to address the VGI error in the fluid phase where the node-type switching is absent. In this scheme, the distribution functions at the boundary nodes are transformed from a fixed coordinate system to a moving coordinate system before the bounce back is implemented. Then, the post bounce-back distribution functions at the boundary nodes are transformed back to the fixed coordinate system. This coordinate transformation treatment can be easily combined with the existing interpolated bounce-back schemes to maintain the desired accuracy of the LBM simulations. The force evaluation method is also modified to satisfy Newton's Third Law.

4. The new bounce back scheme is tested in three benchmark cases, a Poiseuille flow between two inclined straight walls, a turbulent channel flow and finally, a turbulent pipe flow. Compared with the existing bounce back schemes, the new bounce back scheme can significantly improve the accuracy of the simulated flow velocity in both laminar and turbulent flows.

5. The additional computational brought by the use of the new bounce back over its original scheme is negligibly small, typically only around 1%.

It is hoped that the results in this study can generate a renewed interest in re-visiting rigorous implementation issues in LBM associated with a moving curved boundary, specifically, the enforcement of the Galilean invariance and Newton's Third Law at the fluid-solid interface. The LBM method can become a very accurate CFD tool if unexpected issues such as those associated with a general moving solid surface, recognized and treated in this study, can be fully understood. Other methods could be developed to ensure the simultaneous Galilean invariance of the simulated force on the moving solid boundary and the resulting fluid flow.

Finally, we stress that the current study only consider the case where the solid boundary is moving along a fixed line (in 2D) or a fixed surface (in 3D). The case of freely moving fluid-solid surface should be re-examined. In particular, the consideration of full Galilean invariance requirement outlined in this paper may help remove the often-encountered oscillations of resulting hydrodynamic force on the solid body [24]. However, how to improve the implementation for that case remains an open question.

[1] A. J. Ladd. Numerical simulations of particulate suspensions via a discretized boltzmann equation. part 1. theoretical foundation. *Journal of Fluid Mechanics*, 271(1):285–309, 1994.
[2] C. K. Aidun, Y. Lu, E.-J. Ding, et al. Direct analysis of particulate suspensions with inertia using the discrete boltzmann equation. *Journal of Fluid Mechanics*, 373(1):287–311, 1998.

[3] A. Ten Cate, J. J. Derksen, L. M. Portela, and H. E. Van Den Akker. Fully resolved simulations of colliding monodisperse spheres in forced isotropic turbulence. *J. Fluid Mech*, 519:233–271, 2004.

[4] H. Gao, H. Li, and L.-P. Wang. Lattice boltzmann simulation of turbulent flow laden with finite-size particles. *Computers & Mathematics with Applications*, 65(2):194–210, 2013.

[5] D. Yu, R. Mei, L.-S. Luo, and W. Shyy. Viscous flow computations with the method of lattice boltzmann equation. *Progress in Aerospace Sciences*, 39(5):329–367, 2003.

[6] I. Ginzburg and D. dHumières. Multireflection boundary conditions for lattice boltzmann models. *Physical Review E*, 68(6):066614, 2003.

[7] C. Pan, L.-S. Luo, and C. T. Miller. An evaluation of lattice boltzmann schemes for porous medium flow simulation. *Computers & fluids*, 35(8):898–909, 2006.

[8] M. Bouzidi, M. Firdaouss, and P. Lallemand. Momentum transfer of a boltzmann-lattice fluid with boundaries. *Physics of Fluids (1994-present)*, 13(11):3452–3459, 2001.

[9] R. Mei, W. Shyy, D. Yu, and L.-S. Luo. Lattice boltzmann method for 3-d flows with curved boundary. *Journal of Computational Physics*, 161(2):680–699, 2000.

[10] R. Mei, D. Yu, W. Shyy, and L.-S. Luo. Force evaluation in the lattice boltzmann method involving curved geometry. *Physical Review E*, 65(4):041203, 2002.

[11] H. Li, H. Fang, Z. Lin, S. Xu, and S. Chen. Lattice boltzmann simulation on particle suspensions in a two-dimensional symmetric stenotic artery. *Physical review E*, 69(3):031919, 2004.

[12] A. Caiazzo and M. Junk. Boundary forces in lattice boltzmann: Analysis of momentum exchange algorithm. *Computers & Mathematics with Applications*, 55(7):1415–1423, 2008.

[13] J. R. Clausen and C. K. Aidun. Galilean invariance in the lattice-boltzmann method and its effect on the calculation of rheological properties in suspensions. *International Journal of Multiphase Flow*, 35(4):307–311, 2009.

[14] Y. Chen, Q. Cai, Z. Xia, M. Wang, and S. Chen. Momentum-exchange method in lattice boltzmann simulations of particle-fluid interactions. *Physical Review E*, 88(1):013303, 2013.

[15] B. Wen, C. Zhang, Y. Tu, C. Wang, and H. Fang. Galilean invariant fluid–solid interfacial dynamics in lattice boltzmann simulations. *Journal of Computational Physics*, 266:161–170, 2014.

[16] S. Krithivasan, S. Wahal, and S. Ansumali. Diffused bounce-back condition and refill algorithm for the lattice boltzmann method. *Physical Review E*, 89(3):033313, 2014.

[17] S. Hou, Q. Zou, S. Chen, G. D. Doolen, and A. C. Cogley. Simulation of cavity flow by the lattice boltzmann method. *arXiv preprint comp-gas/9401003*, 1994.

[18] M. Junk, A. Klar, and L.-S. Luo. Asymptotic analysis of the lattice boltzmann equation. *Journal of Computational Physics*, 210(2):676–704, 2005.

[19] W.-A. Yong, L.-S. Luo, et al. Accuracy of the viscous stress in the lattice boltzmann equation with simple boundary conditions. *Physical Review E*, 86(6):065701, 2012.

[20] P. Lallemand and L.-S. Luo. Theory of the lattice boltzmann method: Dispersion, dissipation, isotropy, galilean invariance, and stability. *Physical Review E*, 61(6):6546, 2000.

[21] J. Latt, B. Chopard, O. Malaspinas, M. Deville, and A. Michler. Straight velocity boundaries in the lattice boltzmann method. *Physical Review E*, 77(5):056703, 2008.

[22] Z.-G. Feng and E. E. Michaelides. The immersed boundary-lattice boltzmann method for solving fluid–particles interaction problems. *Journal of Computational Physics*, 195(2):602–628, 2004.

[23] Y. Peng and L.-S. Luo. A comparative study of immersed-boundary and interpolated bounce-back methods in lbe. *Progress in Computational Fluid Dynamics, an International Journal*, 8(1-4):156–167, 2008.

[24] C. Peng, Y. Teng, B. Hwang, Z. Guo, and L.-P. Wang. Implementation issues and benchmarking of lattice boltzmann method for moving rigid particle simulations in a viscous flow. *Computers & Mathematics with Applications*, 72(2):349–374, 2016.

[25] S. Tao, J. Hu, and Z. Guo. An investigation on momentum exchange methods and refilling algorithms for lattice boltzmann simulation of particulate flows. *Computers & Fluids*, 133:1–14, 2016.

[26] B. Wen, C. Zhang, and H. Fang. Hydrodynamic force evaluation by momentum exchange method in lattice boltzmann simulations. *Entropy*, 17(12):8240–8266, 2015.

[27] X. He and L.-S. Luo. Lattice boltzmann model for the incompressible navier–stokes equation. *Journal of statistical Physics*, 88(3-4):927–944, 1997.

[28] H. Fang, Z. Wang, Z. Lin, and M. Liu. Lattice boltzmann method for simulating the viscous flow in large distensible blood vessels. *Physical Review E*, 65(5):051925, 2002.

[29] P. Lallemand and L.-S. Luo. Lattice boltzmann method for moving boundaries. *Journal of Computational Physics*, 184(2):406–421, 2003.

[30] A. Caiazzo. Analysis of lattice boltzmann nodes initialisation in moving boundary problems. *Progress in Computational Fluid Dynamics, an International Journal*, 8(1-4):3–10, 2008.

[31] R. Zhang, C. Sun, Y. Li, R. Satti, R. Shock, J. Hoch, and H. Chen. Lattice boltzmann approach for local reference frames. *Communications in Computational Physics*, 9(05):1193–1205, 2011.

[32] M. Meldi, E. Vergnault, and P. Sagaut. An arbitrary lagrangian–eulerian approach for the simulation of immersed moving solids with lattice boltzmann method. *Journal of Computational Physics*, 235:182–198, 2013.

[33] L.-P. Wang, C. Peng, Z. Guo, and Z. Yu. Lattice boltzmann simulation of particle-laden turbulent channel flow. *Computers & Fluids*, 124:226 – 236, 2016. Special Issue for ICMMES-2014.

[34] J. Kim, P. Moin, and R. Moser. Turbulence statistics in fully developed channel flow at low reynolds number. *Journal of*

Fluid Mechanics, 177:133–166, 4 1987.

[35] J. Jimenez and S. Hoyas. Turbulent fluctuations above the buffer layer of wall-bounded flows. *Journal of Fluid Mechanics*, 611:215–236, 9 2008.

[36] P. Loulou, R. D. Moser, N. N. Mansour, and *et al.* Direct numerical simulation of incompressible pipe flow using a B-spline spectral method. *NASA Tech. Memo.*, No. 110436, 1997, 1997.